HHS Public Access

Author manuscript

Curr Biol. Author manuscript; available in PMC 2019 August 06.

Published in final edited form as:

Curr Biol. 2018 August 06; 28(15): 2388–2399.e5. doi:10.1016/j.cub.2018.05.094.

AMPK-mediated BECN1 phosphorylation Promotes Ferroptosis by Directly Blocking System X_c^- Activity

Xinxin Song[1,2], **Shan Zhu**[1], **Pan Chen**[2], **Wen Hou**[2], **Qirong Wen**[1], **Jiao Liu**[1], **Yangchun Xie**[2,3], **Jinbao Liu**[1], **Daniel J. Klionsky**[4], **Guido Kroemer**[5,6,7,8,9,10,11], **Michael T. Lotze**[2], **Herbert J. Zeh**[2], **Rui Kang**[2], and **Daolin Tang**[1,2,12,*]

[1]The Third Affiliated Hospital, Center for DAMP Biology, Key Laboratory for Major Obstetric Diseases of Guangdong Province, Key Laboratory of Protein Modification and Degradation of Guangdong Higher Education Institutes, Key Laboratory of Reproduction and Genetics of Guangdong Higher Education Institutes, School of Basic Medical Sciences, Guangzhou Medical University, Guangzhou, Guangdong, 510510, China

[2]Department of Surgery, University of Pittsburgh, Pittsburgh, Pennsylvania 15213, USA

[3]Department of Oncology, The Second Xiangya Hospital of Central South University, Changsha, Hunan 410008, China

[4]Life Sciences Institute and Department of Molecular, Cellular and Developmental Biology, University of Michigan, Ann Arbor, MI 48109, USA

[5]Université Paris Descartes, Sorbonne Paris Cité; 75006 Paris, France

[6]Equipe 11 labellisée Ligue Nationale contre le Cancer, Centre de Recherche des Cordeliers; 75006 Paris, France

[7]Institut National de la Santé et de la Recherche Médicale, U1138; Paris, France

[8]Université Pierre et Marie Curie, 75006 Paris, France

[9]Metabolomics and Cell Biology Platforms, Gustave Roussy Cancer Campus; 94800 Villejuif, France

[10]Pôle de Biologie, Hôpital Européen Georges Pompidou, AP-HP; 75015 Paris, France

[11]Department of Women's and Children's Health, Karolinska University Hospital, 17176 Stockholm, Sweden

[*]Correspondence to: Daolin Tang (tangd2@upmc.edu).
[12]Lead contact

Author Contributions

D.T. and X.S. designed the experiments. X.S., S.Z., Y.X., Q.W., P.C., J.L, W.H., R.K., and D.T. conducted the experiments. G.K., J.L., D.J.K., M.T.L, H.J.Z, R.K., and D.T analyzed the data. X.S. and D.T. wrote the paper. G.K., J.L., D.J.K., M.T.L., and H.J.Z. edited and commented on the manuscript.

Declaration of Interests

The authors declare no conflicts of interest or financial interests.

Summary

Ferroptosis is a form of regulated cell death triggered by lipid peroxidation after inhibition of the cystine/glutamate antiporter system X_c^-. However, key regulators of system X_c^- activity in ferroptosis remain undefined. Here, we show that BECN1 plays a hitherto unsuspected role in promoting ferroptosis through directly blocking system Xc^- activity via binding to its core component, SLC7A11 (solute carrier family 7 member 11). Knockdown of BECN1 by shRNA inhibits ferroptosis induced by system X_c^- inhibitors (e.g., erastin, sulfasalazine, and sorafenib), but not other ferroptosis inducers including RSL3, FIN56, and buthionine sulfoximine. Mechanistically, AMP-activated protein kinase (AMPK)-mediated phosphorylation of BECN1 at Ser90/93/96 is required for BECN1-SLC7A11 complex formation and lipid peroxidation. Inhibition of PRKAA/AMPKα by siRNA or compound C diminishes erastin-induced BECN1 phosphorylation at S93/96, BECN1-SLC7A11 complex formation, and subsequent ferroptosis. Accordingly, a BECN1 phosphorylation-defective mutant (S90,93,96A) reverses BECN1-induced lipid peroxidation and ferroptosis. Importantly, genetic and pharmacological activation of the BECN1 pathway by overexpression of the protein in tumor cells or by administration of the BECN1 activator peptide Tat-beclin 1, respectively, increases ferroptotic cancer cell death (but not apoptosis and necroptosis) *in vitro* and *in vivo*, in subcutaneous and orthotopic tumor mouse models. Collectively, our work reveals that BECN1 plays a novel role in lipid peroxidation that could be exploited to improve anticancer therapy by the induction of ferroptosis.

eTOC Blurb

Song et al. find that BECN1 promotes ferroptosis by directly blocking system Xc^- activity via binding to its core component SLC7A11. This pathway is different from the previously identified function of BECN1 as a positive regulator of autophagy via directly activating PtdIns3K activity via binding to its core component PIK3C3.

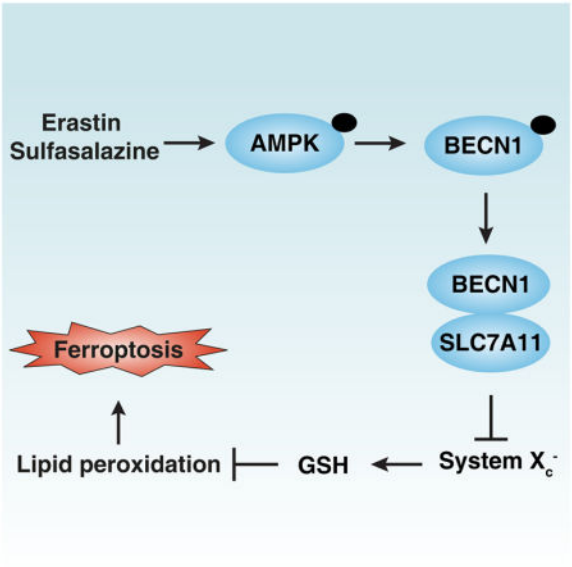

Keywords

autophagy; BECN1; ferroptosis; lipid peroxidation; SLC7A11; autosis

Introduction

System X_c^- is a heterodimeric cystine/glutamate antiporter and is composed of two core components: SLC7A11 (solute carrier family 7 member 11; the catalytic subunit) and SLC3A2 (solute carrier family 3 member 2; an anchoring protein). This amino acid antiporter plays a role in maintaining an intracellular reducing environment by importing cystine, which is reduced to cysteine and then used to synthesize the major antioxidant glutathione (GSH). Impairment of the system X_c^--dependent antioxidant defense system results in oxidative injury and cell death. In particular, pharmacological inhibition of system X_c^- activity by certain small molecule compounds or drugs (e.g., erastin, sulfasalazine, and sorafenib) can trigger ferroptosis, a lipid peroxidation-dependent form of non-apoptotic regulated cell death [1–3]. However, key regulators of system X_c^- activity in ferroptosis remain undefined.

BECN1 (beclin 1) is a key player of macroautophagy/autophagy because it is the central constituent of the class III phosphatidylinositol 3-kinase (PtdIns3K) complex [4, 5]. In addition to binding to core components or regulators of the PtdIns3K complex (e.g., PIK3C3 [phosphatidylinositol 3-kinase catalytic subunit type 3], ATG14 [autophagy related 14], and UVRAG [UV radiation resistance associated]), BECN1 can interact with additional protein partners to regulate various cell processes (e.g., endocytosis and phagocytosis) in both autophagy-dependent and -independent manners [6–8]. To uncover the pleiotropic function of BECN1, it is important to explore the stress-induced changes in the composition of the BECN1 interactome, as well as the post-translational modification (PTMs) occurring within distinct BECN1 complexes.

Here we report that BECN1 plays a non-autophagic role in promoting ferroptosis by binding to SLC7A11. Notably, AMP-activated protein kinase (AMPK)-mediated phosphorylation of BECN1 at Ser90/93/96 is required for BECN1-SLC7A11 complex formation and subsequent lipid peroxidation in ferroptosis. Thus, BECN1 contributes to the core molecular machinery and signaling pathways involved in ferroptosis.

Results

BECN1 is required for system X_c^- inhibitor-induced ferroptosis

To determine the role of BECN1 in ferroptosis, BECN1 protein expression was measured in human cancer cell lines including HCT116 (colon adenocarcinoma), CX-1 (colon adenocarcinoma), PANC1 (pancreatic ductal adenocarcinoma), HT1080 (fibrosarcoma), and Calu-1 (non-small-cell lung cancer) cells. Consistent with previous studies showing that ferroptosis is associated with increased autophagy [9, 10], erastin (a classical inducer of ferroptosis) induced the conversion of the autophagic marker MAP1LC3B (microtubule associated protein 1 light chain 3 beta)-I to -II, as determined by immunoblot analysis

(Figure 1A) and increased the formation of MAP1LC3B puncta formation, as determined by immunofluorescence staining and image analysis (Figure S1A and S1B). Normal cell culture condition did not induce MAP1LC3B-II expression in PANC1 and Calu-1 cells after 24 hours culture (Figure S1C). In addition to erastin-induced BECN1 expression in HT1080 cells, there were no significant changes in the protein expression of BECN1 in other cell lines (Figure 1A), indicating that the inducible expression of BECN1 may not be essential for erastin-induced autophagosome formation.

Next, we investigated the possibility that the expression of BECN1 might affect the anticancer activity of system X_c^- inhibitors (e.g., erastin, sulfasalazine, and sorafenib) in HCT116, CX-1, and HT1080 cells. Transfection-enforced overexpression of *BECN1* (Figure 1B) sensitized cancer cells to system X_c^- inhibitor-induced death (Figure 1C). Conversely, depletion of BECN1 by short hairpin RNA (shRNA)-mediated RNA interference (Figure 1D) conferred resistance to system X_c^- inhibitors (Figure 1E). Moreover, knockdown of BECN1 by means of two additional, non-overlapping shRNAs (Figure S2A) inhibited cell death induced by erastin, sulfasalazine, and sorafenib in HCT116 and HT1080 cells (Figure S2B). Propidium iodide staining confirmed that knockdown of BECN1 inhibited erastin and sulfasalazine-induced cell death in HT1080 cells (Figure S2C). In contrast, alterations of BECN1 expression did not affect cell death induced by other ferroptosis inducers including GPX4 (glutathione peroxidase 4) inhibitor (RSL3 and FIN56) and GSH synthase inhibitor (buthionine sulfoximine [BSO]) (Figure 1C, 1E, and S2B). Of note, knockdown of BECN2 (a paralog of BECN1 [11]) by siRNA (Figure 1F) did not change the anticancer activity of erastin, sulfasalazine, and sorafenib (Figure 1G) in HeLa cells. Thus, the expression of BECN1 selectively contributes to the anticancer activity of those ferroptosis inducers that target system X_c^-, but not those that act downstream of system X_c^-.

Given that BECN1 is also involved in the regulation of apoptosis and other types of regulated cell death [6], we explored the possibility that these forms of regulated cell death might contribute to the anticancer activity of erastin in BECN1-overexpressing cells. To evaluate this hypothesis, we used various cell death inhibitors. Ferroptosis inhibitors (ferrostatin-1 and liproxstatin-1) restored cell viability in BECN1-overexpressing cells (HCT116, CX-1, and HT1080) cultured with X_c^- inhibitors (Figure S2D). In contrast, Z-VAD-FMK (an apoptosis inhibitor) or necrosulfonamide (a necroptosis inhibitor) (Figure S2D) failed to improve cellular viability in these circumstances. As an internal control, Z-VAD-FMK (but not ferrostatin-1 and liproxstatin-1) inhibited cell death induced by the pro-apoptotic agent staurosporine (Figure S2E), and necrosulfonamide (but not ferrostatin-1) inhibited necroptosis induction by TZC (a combination of TNF [tumor necrosis factor], Z-VAD-FMK, and cycloheximide) (Figure S2F). Collectively, these findings indicate that BECN1 is required for system X_c^- inhibitor-induced ferroptosis.

BECN1 promotes GSH depletion and lipid peroxidation in ferroptosis

Although the function of BECN1 in autophagosome formation is established, several studies have revealed various non-autophagic functions of BECN1 [8]. To distinguish between the autophagy-dependent and -independent roles of BECN1 in ferroptosis, we measured the lipidation and subcellular distribution of MAP1LC3B in BECN1-overexpressing, BECN1-

depleted, and control cells in the absence or presence of erastin. Alterations in BECN1 expression did not affect the erastin-induced formation of lipidated MAP1LC3B (i.e., the generation of MAP1LC3B-II, leading to an increase in its electrophoretic mobility) (Figure 2A) and MAP1LC3B-positive puncta (Figure S4) in HCT116 and CX-1 cell lines. As a positive control, knockdown of *BECN1* inhibited starvation (Hanks balanced salt solution [HBSS])-induced MAP1LC3B-II expression (Figure 2B) in HCT116 and CX-1 cells. Consistent with previous studies [9, 10], knockdown of the autophagic regulator *ATG5* by specific shRNA (Figure S3C) inhibited system X_c^- inhibitor (erastin, sulfasalazine, and sorafenib)-induced cell death (Figure S3D) associated with decreased MAP1LC3B puncta formation (Figure S3E). These findings indicate that system X_c^- inhibitor-induced MAP1LC3B lipidation requires ATG5 but not BECN1.

Because lipid peroxidation is a critical driver of ferroptosis [1, 2], we next hypothesized that BECN1-mediated ferroptosis is associated with increased lipid peroxidation. Erastin- or sulfasalazine-induced lipid peroxidation, assessed by means of the fluorescent biosensor C11-BODIPY or by quantifying the oxidative stress marker malondialdehyde (MDA), was increased after overexpression of *BECN1*, but decreased after knockdown of *BECN1* in HCT116 (Figure 2C), CX-1 (Figure S3F), and HT1080 cells (Figure S3G). In contrast, erastin- or sulfasalazine-induced accumulation of Fe^{2+}, assessed by means of the Iron Assay Kit, was not significantly affected by BECN1 expression (Figure 2C, S3F and S3G). Intracellular chelatable iron was further determined using the fluorescent indicator Phen Green SK, the fluorescence of which is quenched by iron [12]. Erastin-induced downregulation of the proportion of Phen Green SK-positive cells was not affected by knockdown of BECN1 in HT1080 cells (Figure 2D). Moreover, erastin-induced iron metabolism-associated genes (e.g., *FTH1* [ferritin heavy chain 1], *FTL* [ferritin light chain], *TFRC* [transferrin receptor], *SLC11A2/DMT1* [solute carrier family 11 member 2/divalent metal transporter 1], and *SLC40A1/FPN1* [solute carrier family 40 member 1/ferroportin 1]) mRNA expression were not affected by knockdown of BECN1 in HT1080 cells (Figure 2E). These findings suggest that BECN1 promotes system X_c^- inhibitor-induced ferroptosis through upregulation of lipid peroxidation, but not iron accumulation.

Given that GSH levels inversely correlate with lipid peroxidation [13], we hypothesized that the increased lipid peroxidation in *BECN1*-overexpressing cancer cells should be associated with reduced GSH levels in ferroptosis. Indeed, overexpression of *BECN1* increased GSH depletion, whereas depletion of *BECN1* restored GSH levels in HCT116 (Figure 2C), CX-1 (Figure S3F), and HT1080 (Figure S3G) cells following erastin or sulfasalazine treatment. Moreover, the administration of GSH inhibited erastin- or sulfasalazine-induced death with increased intracellular GSH levels in wild-type and BECN1-overexpressing HCT116 cells (Figure 2F). These findings indicate that BECN1 promotes GSH depletion and lipid peroxidation in system X_c^- inhibitor-induced ferroptosis.

BECN1 inhibits system Xc⁻ activity through direct binding to SLC7A11

Previous studies have demonstrated that erastin not only inhibits system Xc^- activity to trigger ferroptosis, but also upregulates the expression of SLC7A11 (the catalytic subunit of system Xc^-) as a negative feedback loop to limit lipid peroxidation [3, 14]. We therefore

investigated whether BECN1 alters the expression and activity of system Xc^- to modulate GSH level and ferroptosis. BECN1 expression did not affect the erastin-induced *SLC7A11* mRNA upregulation in HCT116 and CX-1 cells (Figure S4A). In contrast, a glutamate release assay indicated that the activity of system Xc^- was inhibited in BECN1-overexpressing cells, whereas it was increased in BECN1-knockdown HCT116 and CX-1 cells following erastin treatment (Figure 3A). These findings suggest that BECN1 inhibits system Xc^- activity, but not SLC7A11 expression.

Because BECN1 serves as a protein interaction platform [6–8], we next asked whether BECN1 inhibits system Xc^- activity through direct protein-protein interactions. Immunoprecipitation (IP) of cellular lysates by means of an anti-BECN1 or anti-SLC7A11 antibody followed by immunoblot detection of SLC7A11 or BECN1 revealed a significant BECN1-SLC7A11 interaction in HCT116 and/or CX-1 cells following erastin treatment (Figure 3B). Moreover, the erastin-induced BECN1-SLC7A11 complex was more abundant in BECN1-overexpressing HCT116 and CX-1 cells (Figure 3B). A similar phenomenon was further confirmed by IP assay using anti-HA tag antibody in HCT116 and CX-1 cells expressed HA-BECN1 (Figure 3C). The formation of a BECN1-SLC7A11 complex also occurred in PANC1, HT1080, and Calu-1 cells following erastin or sulfasalazine treatment (Figure 3D). Image assay showed that the colocalization between BECN1 and SLC7A11 occurs mostly in the cytoplasm in CX-1 cells following erastin treatment (Figure 3E). Moreover, the BECN1 activator peptide Tat-beclin 1 (H_2N-YGRKKRRQRRR-GG-TNVFNATFEIWHDGEFGT-CO_2H) [15] increased BECN1-SLC7A11 complex formation (Figure 3F), the inhibition of glutamate release (Figure 3G), and subsequent cell death in HCT116 cells following erastin or sulfasalazine treatment (Figure 3H). These findings indicate that the formation of the BECN1-SLC7A11 complex inhibits system Xc^- activity in ferroptosis.

Of note, the increased BECN1-SLC7A11 complex was not observed in starvation (HBSS)-induced autophagy (Figure S4B), although starvation did induce formation of the BECN1-PIK3C3 complex, as expected [6]. However, erastin did not induce the BECN1-PIK3C3 interaction (Figure S4B). These observations suggest that SLC7A11 and PIK3C3 form mutually exclusive complexes with BECN1 in the context of ferroptosis and classical autophagy, respectively.

BECN1 phosphorylation at S90/93/96 contributes to BECN1-SLC7A11 complex formation

Human BECN1 has 450 amino acids (aa), including three domains: a BH3 domain at the N terminus, a central coiled-coil domain (CCD), and a C-terminal half encompassing the evolutionarily conserved domain (ECD) that is present within the BARA domain [6]. To define the portions of the BECN1 protein responsible for the interaction with SLC7A11, we constructed a series of vectors that express fragments of BECN1 (1-150, 1-242, 151-241, and 243-450). IP assays showed that the aa 1-150 fragment of BECN1 can bind to SLC7A11 (Figure 4A). Compared to full-length BECN1, functional assays further demonstrated that aa 1-150 of BECN1 had the same ability to enhance erastin- or sulfasalazine-induced cell death and to concomitantly increase MDA production and deplete GSH (Figure 4B). In contrast,

aa 243-450 of BECN1 failed to enhance erastin- or sulfasalazine -induced cell death and lipid peroxidation (Figure 4B).

The BECN1 interactome is profoundly influenced through BECN1 phosphorylation by various kinases [16]. We therefore mutated putative phosphorylation sites in BECN1 by replacing serine (S) or threonine (T) residues to alanine (A) in aa 1-150 (S15A, S30A, S90A, T108A, T119A, and S90,93,96A). Moreover, we specifically deleted the BH3 domain (114-128), knowing that this domain is important for inhibitory interactions with BCL2 and BCL2L1 [17]. IP assays showed that only the S90,93,96A mutant (but not any other Ser/Thr mutants nor the BH3 domain deletion) attenuated the interaction with SLC7A11 in erastin-induced ferroptosis (Figure 4C). Moreover, in contrast to full-length BECN1 and other phosphorylation mutants, the S90,93,96A mutant failed to enhance erastin- or sulfasalazine-induced cell death, MDA production, and GSH depletion (Figure 4D). Iron accumulation was not affected by any of these phosphorylation mutants (Figure 4D). Collectively, these findings demonstrate that the phosphorylation of BECN1 at S90/93/96 contributes to BECN1-SLC7A11 complex formation and subsequent lipid peroxidation in ferroptosis.

AMPK is required for BECN1 phosphorylation in ferroptosis

It has been reported that AMP-activated protein kinase (AMPK) phosphorylates BECN1 at S90 and S93 to regulate autophagy or cell trafficking [18]. Erastin time-dependently increased BECN1 phosphorylation at S90 and S93, as well as the activating PRKAA/AMPKα phosphorylation at Thr172 in HCT116 and CX-1 cells (Figure 5A). To establish a direct link between PRKAA/AMPKα and BECN1, we next sought to clarify whether inhibition of PRKAA/AMPKα expression or activity might suppress BECN1 phosphorylation and BECN1-SLC7A11 complex formation in ferroptosis. Genetic or pharmacological inhibition of PRKAA/AMPKα by siRNA or by compound C, respectively, diminished erastin-induced BECN1 phosphorylation at S93/96 (Figure 5B and 5C) as well as BECN1-SLC7A11 complex formation (Figure 5D and 5E) in HCT116 and CX-1 cells. Pharmacological application of Compound C may result in both AMPK-dependent and -independent effects in different contexts [19]. Similar to previous studies [3, 14], erastin increased SLC7A11 expression (Figure 5D). Unlike knockdown of PRKAA/AMPKα (Figure 5D), compound C increased SLC7A11 expression in HCT116 cells (Figure 5E), indicating that AMPK-independent effects of compound C regulate SLC7A11 expression. Consequently, knockdown of PRKAA/AMPKα or administration of compound C (Figure 5F and 5G) suppressed erastin- or sulfasalazine-induced death with decreased MDA production and increased GSH levels in HCT116 (Figure 5F and 5G) and CX-1 cells (Figure S5). Again, iron accumulation was not changed by the genetic and pharmacological inhibition of AMPK (Figure 5F, 5G, and S9). Collectively, these findings support the hypothesis that PRKAA/AMPKα-mediated BECN1 phosphorylation promotes BECN1-SLC7A11 complex formation and subsequent lipid peroxidation in ferroptosis.

BECN1 contributes to the anticancer activity of ferroptosis in vivo

We investigated whether overexpression of BECN1 enhances the anticancer activity of erastin *in vivo.* BECN1-overexpressing and control HCT116 cells were implanted subcutaneously into the right flank of immunodeficient nude mice. One week later, tumor-

bearing mice were treated with erastin for two weeks. Compared with control wild-type cells, erastin effectively reduced the tumor growth of BECN1-overexpressing HCT116 cells (Figure 6A–6C), as it locally augmented MDA levels and diminished GSH levels without altering erastin-induced Fe^{2+} accumulation (Figure 6D). A similar anticancer activity of erastin and phenotypic alterations in GSH and MDA (but not Fe^{2+}) was observed in nude mice after subcutaneous implantation of BECN1-overexpressing (but not control) CX-1 cells (Figure S6). In contrast, overexpression of BECN1 did not change the protein levels of cleaved CASP3/caspase 3 (a marker of apoptosis) and phosphorylation of MLKL (mixed lineage kinase domain like pseudokinase, a marker of necroptosis) with or without erastin treatment *in vivo* (Figure 6E). These data indicate that BECN1 expression sensitizes to erastin-induced lipid peroxidation, ferroptosis, and tumor suppression *in vivo*.

We next investigated whether the BECN1 activator peptide Tat-beclin 1 enhances the anticancer activity of erastin in mouse tumor models. Tat-beclin 1 increased the anticancer activity of erastin in immunodeficient nude mice after subcutaneous implantation of HCT116 or HT1080 cells (Figure 6F). Like overexpression of BECN1 (Figure 6E), administration of Tat-beclin 1 did not change the protein levels of cleaved CASP3 and phosphorylation of MLKL with or without erastin treatment *in vivo* (Figure 6G). Furthermore, Tat-beclin 1 combined with erastin was more efficient than erastin alone in increasing animal survival in an orthotopic pancreas cancer (KPC) model (Figure 6H). Liproxstatin-1 (an inhibitor of ferroptosis) blocked the anticancer activity of erastin combined with Tat-beclin 1 in these animal models (Figure 6F and 6H). Altogether, these results further support the idea that activation of the BECN1 pathway effectively enhances the anticancer activity of erastin by induction of ferroptosis, but not apoptosis or necroptosis.

Discussion

In this study, we reported that BECN1 plays a new role in the control of system Xc^- activity, which is critical for ferroptosis induction. Mechanistically, phosphorylation of BECN1 at Ser90/93/96 by PRKAA/AMPKα contributes to the formation of a BECN1-SLC7A11 complex and system Xc^- inhibition. Consequently, activation of BECN1 promotes GSH depletion and lipid peroxidation in tumor suppression.

The term “ferroptosis” was first coined in 2012 and was largely based on the observation of an iron-dependent form of nonapoptotic cell death in cancer cells triggered by erastin [3]. In addition to its potential utility in cancer therapy [20–27], ferroptosis may represent an inflammatory cell death involved in tissue injury and immune regulation [28–33]. The mechanism of erastin-induced ferroptosis is still not fully understood at the molecular level, although it is well known that it requires the RAS-RAF-MAP2K/MEK-MAPK//ERK signaling cascade and is highly cell specific [34]. In recent years, accumulating evidence indicates that lipid peroxidation plays a central role in the initiation and progression of ferroptosis. In particular, pharmacological inhibition of system Xc^- leads to lipid peroxidation and ferroptosis [35]. Our results indicate that the system Xc^- inhibitors erastin or sulfasalazine promote BECN1 binding to SLC7A11 as an early step to initiate ferroptosis. This negative feedback step seems to be an important regulatory mechanism for limiting system Xc^- activity following the upregulation of SLC7A11 expression. Inhibition of

SLC7A11 expression at the transcriptional level is an alternative strategy to inhibit system Xc^- activity and consequently enhance ferroptosis [14, 36]. Thus, there are least two modes, transcription-independent (protein-protein interaction) and transcription-dependent, for the control of system Xc^- activity in ferroptosis.

A rich collection of literature has demonstrated the critical tie between autophagy, survival, and cell death, but why, how, and when autophagy switches from pro-survival to lethal functions is still under debate [37–39]. Autophagy involves dynamic and complicated processes and can occur using multiple variant mechanisms dependent or independent of core ATG proteins. Our current study indicates that BECN1-independent autophagy positively regulates system Xc^- inhibitor-induced, but not GPX4 inhibitor-induced ferroptosis. Similarly, BECN1 is not required for apoptosis induction (e.g., by staurosporine, gossypol, and resveratrol) or for cis-unsaturated fatty acid-induced autophagy in certain cancer cells [40, 41].

Dynamic changes in the BECN1 interactome play a major role in the crosstalk between cell death and autophagy regulatory pathways. As a central platform of this interaction hub, BECN1 may affect a lethal signal transduction pathway through autophagy-dependent and independent mechanisms [6–8]. Contrasting with the central pro-autophagic BECN1 function, which includes the interaction with PIK3C3 to form class III PtdIns3K complex, we demonstrated here that BECN1 promotes ferroptosis through interaction with SLC7A11. The structural basis of the regulation of the formation of different BECN1 complexes has partially been elucidated. For example, the BH3 domain of BECN1 mediates binding to BCL2 family proteins such as BCL2 itself and BCL2L1, the CCD domain interacts with UVRAG, and the ECD domain contributes to interaction with lipid membranes [42–44]. Our experimental evidence shows that aa 1-150 of BECN1 are required for BECN1-SLC7A11 formation in ferroptosis. Moreover, phosphorylation of BECN1 at S90/93/96 by AMPK increases binding to SLC7A11, meaning that AMPK inhibition and mutation of S90/93/96 to render these residues non-phosphorylable, compromised the pro-ferroptotic function of BECN1. Of note, AMPK-mediated BECN1 phosphorylation at T388 promotes BECN1-PIK3C3 complex formation in autophagy [45]. At present, however, we do not understand which additional signals acting on BECN1 (beyond AMPK activation) determine whether the protein will preferentially engage in BECN1-SLC7A11 or BECN1-PIK3C3 complexes to stimulate ferroptosis and autophagy, respectively.

It is interesting to note that genetic or pharmacological activation of BECN1 enhanced the anticancer activity of erastin in multiple preclinical animal tumor models. In particular, a BECN1 activator peptide enhanced BECN1-SLC7A11 complex formation and lipid peroxidation *in vitro* and/or *in vivo*. The BECN1 activator peptide has previously been reported to trigger autophagic cell death in fibroblasts and HeLa cancer cells independent of apoptosis or necroptosis [15]. We and others have recently demonstrated that ferroptosis is an autophagic cell death process [9, 10], supporting the crosstalk between autophagy and different forms of regulated cell death in cancer therapy. Although the half-life of erastin is relatively short *in vivo*, it exhibits anticancer activity in multiple mouse models [26, 46], indicating that unknown metabolites produced from erastin may mediate anticancer activity.

In summary, we define a regulatory signaling pathway mediated by BECN1 that positively controls ferroptosis through directly blocking system Xc^- activity. This BECN1-dependent pathway may represent a potential target for the development of pharmacological agents that enhance or inhibit ferroptotic signaling pathways.

STAR★METHODS

CONTACT FOR REAGENT AND RESOUCE SHARING

Further information and requests for resources and reagents should be directed to and will be fulfilled by the Lead Contact, Daolin Tang (tangd2@upmc.edu).

EXPERIMENTAL MODEL AND SUBJECT DETAILS

Mice—To generate murine subcutaneous tumors, 5×10^6 HCT116, CX-1, or HT1080 cells in 100 μl phosphate buffered saline (PBS; Thermo Fisher Scientific, AM9625) were injected subcutaneously right of the dorsal midline in athymic nude immunodeficient mice (six- to eight-week-old, female). To generate orthotopic tumors, 1×10^6 KPC cells in 10 μl PBS were surgically implanted into the pancreases of immunocompetent C57BL/6J mice (six- to eight-week-old, female) [47, 48]. All animal experiments were approved by the Institutional Animal Care and Use Committees and performed in accordance with the Association for Assessment and Accreditation of Laboratory Animal Care guidelines (http://www.aaalac.org). Mice were health checked daily throughout the experiment and kept on a regular 12 hr light and dark cycle with normal diet in a pathogen-free barrier facility. Mice were not involved in previous procedures and test naïve.

Cell Culture—The HCT116 (CCL-247, male), PANC1 (CCL-1469, male), HT1080 (CCL-121, male), Calu-1 (HTB-54, male), HeLa (CCL-2, female), and HEK293T (CRL-3216) cell lines were obtained from American Type Culture Collection (ATCC). Sex information of HEK293T cell line was unavailable from ATCC. The CX-1 cell line (male) was a gift from Dr. Yong Lee (University of Pittsburgh). The mouse PDAC cell line KPC was derived from tumors from male KPC mice (*Pdx1-Cre;K-Ras$^{G12D/+}$;Trp53$^{R172H/+}$*) as previously described [49]. These cells were cultured in Dulbecco's Modified Eagle's Medium (ThermoFisher Scientific, 11995073) or McCoy's 5a Medium (Thermo Fisher Scientific, 16600082) or Minimum Essential Medium (Thermo Fisher Scientific, 11095080) supplemented with 10% heat-inactivated fetal bovine serum (Millipore, TMS-013-B) and 1% penicillin and streptomycin (Thermo Fisher Scientific, 15070-063) at 37 °C, 95% humidity, and 5% CO_2. All cells were mycoplasma-free and authenticated using Short Tandem Repeat DNA Profiling Analysis.

METHOD DETAILS

Cell viability assay—Cells were seeded into 96-well plates and incubated with the indicated treatments. Subsequently, 100 μl fresh medium was added to cells containing 10 μl Cell Counting Kit-8 (CCK-8) solutions (Dojindo Laboratories, CK04) and incubated for 2 h (37°C, 5% CO_2). Absorbance at 450 nm was measured using a microplate reader (Cytation™ 5 Cell Imaging Multi-Mode Reader, BioTek, USA). Propidium iodide staining was used to assay cell death.

Western blot analysis—Cells were lysed with 1X cell lysis buffer (Cell Signaling Technology, 9803) containing protease inhibitor (Sigma-Aldrich, P8340) on ice for 10 min, homogenized by passing through a 21-gauge needle, and centrifuged at 14,000 x g for 15 min at 4°C to pellet the cell debris. Protein was quantified using the BCA assay (Thermo Fisher Scientific, 23225) and 20 μg of each sample was resolved on 4%–12% Criterion XT Bis-Tris gels (Bio-Rad, 3450124) in XT MES running buffer (Bio-Rad, 1610789) and transferred to PVDF membranes (Bio-Rad, 1620233) using the Trans-Blot® Turbo™ Transfer Pack and System (Bio-Rad). Membranes were blocked with TBST (Cell Signaling Technology, 9997S) containing 5% skim milk for 1 h and incubated overnight at 4°C with various primary antibodies. Following 3 washes in TBST, membranes were incubated with goat anti-rabbit or anti-mouse IgG HRP secondary antibody (Cell Signaling Technology, 7074 or 7076) at room temperature for 1 h and washed. Chemiluminescence substrate was applied using SuperSignal™ West Pico Chemiluminescent Substrate (Thermo Fisher Scientific, 34080) or SuperSignal™ West Femto Maximum Sensitivity Substrate (Thermo Fisher Scientific, 34095) and blots were analyzed using the ChemiDoc™ Touch Imaging System (Bio-Rad).

Immunoprecipitation analysis—Cells were lysed at 4°C in ice-cold radioimmunoprecipitation assay buffer (Cell Signaling Technology, 9806) and cell lysates were cleared by brief centrifugation (13,000 g, 15 min). Concentrations of proteins in the supernatant were determined using the BCA assay. Prior to immunoprecipitation, samples containing equal amounts of proteins were pre-cleared with protein A agarose beads (Santa Cruz Biotechnology, sc-2027; 4°C, 3 h), and subsequently incubated with various irrelevant IgG or specific antibodies (5 μg/mL) in the presence of protein A agarose beads for 2 h or overnight at 4°C with gentle shaking. Following incubation, agarose beads were washed extensively with PBS and proteins were eluted by boiling in 2 × sodium dodecyl sulfate sample buffer before sodium dodecyl sulfate polyacrylamide gel electrophoresis.

Immunofluorescence assay—The cells were fixed with 2% PFA and incubated with primary antibodies in PBS with 1% bovine serum albumin overnight at 4°C, followed by washing and application of secondary antibodies. The secondary antibody was Alexa Fluor 488 goat anti-rabbit IgG (Thermo Fisher Scientific, R37116). The cells were counter-stained with DAPI (Thermo Fisher Scientific, H3569). After final washing, sections were protected with cover slips with anti-fading mounting medium sealed with nail polish and stored at 4°C for preservation. Immunofluorescence images were acquired using an AxioObserver Z1 Microscope with Apotome (Carl Zeiss). Quantifications of images were performed by assessing 20X high-power fields per slide and 10 fields per sample in a blinded manner.

BECN1 fragment and mutant construction—Site mutations were introduced into the *BECN1* gene using the QuikChange site-directed mutagenesis kit (Agilent Technologies, 200523). The mutagenesis reactions were conducted using the primers (Table S1) with pcDNA4-Becn1 (Addgene, 24388; deposited by Qing Zhong) as templates. All constructs were confirmed by DNA sequence analysis.

The deletion of aa 114-128 of BECN1 was amplified by PCR using the primers (Table S1) with pcDNA4-Becn1 as a template. Then the PCR products were cloned into

pcDNA4/3XFlag (Addgene, 24388; deposited by Qing Zhong). The deletion of aa 114-128 of the BECN1 sequence was confirmed by DNA sequence analysis.

Lentivirus production and stable transfection—BECN1 was subcloned into pENTER-D-TOPO (Thermo Fisher Scientific, K240020) with an HA tag and sequenced for verification. The expression vector pLenti CMV/HA- pLenti-HA-Becn1 was generated through LR recombination between pENTR/HA-Becn1 and pLenti CMV Puro DEST (Addgene, 17452; deposited by Eric Campeau and Paul Kaufman) with Gateway LR Clonase II enzyme mix (Thermo Fisher Scientific, 11791100). Lentiviral particles were generated by co-transfecting HEK293T cells with 3rd generation packaging mix (Abm, LV053), and pLenti-HA-Becn1. Lentivirus containing supernatant was collected and passed through 0.45-μm filters to isolate the viral particles. After lentiviral transduction, cells were selected with 5 μg/ml puromycin. The expression of the puromycin-resistant clones was identified using western blot.

Quantitative real time polymerase chain reaction assay (Q-PCR)—Total RNA was extracted and purified from cultured cells using the RNeasy Plus Mini Kit (QIAGEN, 74136). The RNA was quantified by determining absorbance at 260 nm. One μg of total RNA from each sample was reverse transcribed into cDNA using the iScript cDNA synthesis kit (Bio-Rad, 170-8891) in a volume of 20 μl. cDNA from cell samples was amplified. Quantitative real time PCR was performed using ssoFast EvaGreen Supermix (Bio-Rad, 172-5204) on the C1000 Touch Thermocycler CFX96 Real Time System (Bio-Rad, Hercules, CA, USA). Analysis was performed using the Bio-Rad CFX Manager software. The primers, which were synthesized and desalted from Sigma-Aldrich, are shown in Table S1.

RNAi and gene transfection—To generate PRKAA/AMPKα knockdown cells, cells were transfected with 103nM of siRNA against *PRKAA1/AMPKα1* and *PRKAA2/AMPKα2* and control siRNA (SIC001) from Sigma-Aldrich. Transfection was performed with Lipofectamine 3000 (Invitrogen, L3000-015). Target sequences for preparing siRNAs of human *PRKAA1/AMPKα1* and *PRKAA2/AMPKα2* are shown in KEY RESOURCES TABLE. Human BECN2 siRNA pools (sc-88199) were purchased from Santa Cruz Biotechnology. pcDNA4-Becn1 (24388) and its fragments plasmids 1-150 (24389), 1-242 (24391), 151-241 (24393), and 243-450 (24392) were purchased from Addgene (deposited by Qing Zhong). Human-Slc7a11-cDNA (EX-U1104-Lv120) was obtained from GeneCopoeia. Human-*BECN1*-shRNA (TRCN0000299864, TRCN0000299789, and TRCN0000299790) and human-*ATG5*-shRNA (TRCN0000151963) were obtained from Sigma-Aldrich.

Glutamate release assay—The release of glutamate from cells into the extracellular medium was detected using an Amplex Red glutamate release assay kit (Thermo Fisher Scientific, A12221). Glutamate release was first normalized to the total cell number determined with the CCK8 kit at the end of the experiment, and then values were expressed as a percentage of no-treatment controls.

GSH assay—The relative GSH concentration in tissue lysates was assessed using a Glutathione Assay Kit (Sigma-Aldrich, CS0260) according to the manufacturer's instructions. Briefly, the measurement of GSH used a kinetic assay in which catalytic amounts (nmoles) of GSH caused a continuous reduction of 5,5′-dithiobis (2-nitrobenzoic acid) to 5-thio-2-nitrobenzoic acid; the formed GSSG was recycled by GSR/glutathione reductase and NADPH. The reaction rate was proportional to the concentration of glutathione up to 2 mM. The yellow product (5-thio-2-nitrobenzoic acid) was measured spectrophotometrically at 412 nm.

Lipid peroxidation assay—The relative MDA concentration in cell or tumor lysates was assessed using a Lipid Peroxidation (MDA) Assay Kit (Abcam, ab118970). Briefly, MDA in the sample reacts with thiobarbituric acid (TBA) to generate a MDA-TBA adduct. The MDA-TBA adduct can be easily quantified colorimetrically (OD=532 nm). In addition, C11-BODIPY dye (Thermo Fisher Scientific, D3861) was used to detect lipid peroxidation in cells. Oxidation of the polyunsaturated butadienyl portion of the dye results in a shift of the fluorescence emission peak from ~590 nm to ~510 nm.

Iron assay—Intracellular ferrous iron level was determined using the iron assay kit from Sigma-Aldrich (MAK025). Intracellular chelatable iron was determined using the fluorescent indicator Phen Green SK from Thermo Fisher Scientific (P-14313) [50]. The fluorescence of Phen Green SK is quenched by iron.

QUANTIFICATION AND STATISTICAL ANALYSIS

Image Lab™ Software (Bio-Rad) was used for relative quantification of western blot bands. In many case, relative expression was calculated by the optical density ratio of protein to ACTB and normalized against the control. Statistical analysis was performed using Prism 7 software. Unpaired Student's t tests were used to compare the means of two groups. One-way Analysis of Variance (ANOVA) was used for comparison among the different groups. When ANOVA was significant, *post hoc* testing of differences between groups was performed using the Least Significant Difference (LSD) test. The Kaplan-Meier method was used to compare differences in mortality rates between groups. A p-value < 0.05 was considered statistically significant.

Supplementary Material

Refer to Web version on PubMed Central for supplementary material.

Acknowledgments

We thank Christine Heiner (Department of Surgery, University of Pittsburgh) for her critical reading of the manuscript. This work was supported by grants from the US National Institutes of Health (R01GM115366, R01CA160417, R01CA211070, and R01GM053396), the Natural Science Foundation of Guangdong Province (2016A030308011), the American Cancer Society (Research Scholar Grant RSG-16-014-01-CDD), the National Natural Science Foundation of China (31671435, 81400132, and 81772508), Guangdong Province Universities and Colleges Pearl River Scholar Funded Scheme (2017), Lin He's Academician Workstation of New Medicine and Clinical Translation (2017), and International Scientific and Technology Cooperation Program of China (2015DFA31490). This project partly utilized University of Pittsburgh Cancer Institute shared resources supported by award P30CA047904. GK is supported by the Ligue contre le Cancer Comité de Charente-Maritime (équipe labelisée); Agence National de la Recherche (ANR) – Projets blancs; ANR under the frame of E-Rare-2, the ERA-

Net for Research on Rare Diseases; Association pour la recherche sur le cancer (ARC); Cancéropôle Ile-de-France; Chancelerie des universités de Paris (Legs Poix), Fondation pour la Recherche Médicale (FRM); the European Commission (ArtForce); the European Research Council (ERC); Fondation Carrefour; Institut National du Cancer (INCa); Inserm (HTE); Institut Universitaire de France; LeDucq Foundation; the LabEx Immuno-Oncology; the RHU Torino Lumière, the Searave Foundation; the SIRIC Stratified Oncology Cell DNA Repair and Tumor Immune Elimination (SOCRATE); the SIRIC Cancer Research and Personalized Medicine (CARPEM); and the Paris Alliance of Cancer Research Institutes (PACRI).

References

1. Xie Y, Hou W, Song X, Yu Y, Huang J, Sun X, Kang R, Tang D. Ferroptosis: process and function. Cell death and differentiation. 2016; 23:369–379. [PubMed: 26794443]
2. Stockwell BR, Friedmann Angeli JP, Bayir H, Bush AI, Conrad M, Dixon SJ, Fulda S, Gascon S, Hatzios SK, Kagan VE, et al. Ferroptosis: A Regulated Cell Death Nexus Linking Metabolism, Redox Biology, and Disease. Cell. 2017; 171:273–285. [PubMed: 28985560]
3. Dixon SJ, Lemberg KM, Lamprecht MR, Skouta R, Zaitsev EM, Gleason CE, Patel DN, Bauer AJ, Cantley AM, Yang WS, et al. Ferroptosis: an iron-dependent form of nonapoptotic cell death. Cell. 2012; 149:1060–1072. [PubMed: 22632970]
4. Liang XH, Jackson S, Seaman M, Brown K, Kempkes B, Hibshoosh H, Levine B. Induction of autophagy and inhibition of tumorigenesis by beclin 1. Nature. 1999; 402:672–676. [PubMed: 10604474]
5. Klionsky DJ. Autophagy: from phenomenology to molecular understanding in less than a decade. Nature reviews. Molecular cell biology. 2007; 8:931–937. [PubMed: 17712358]
6. Kang R, Zeh HJ, Lotze MT, Tang D. The Beclin 1 network regulates autophagy and apoptosis. Cell death and differentiation. 2011; 18:571–580. [PubMed: 21311563]
7. Sinha S, Levine B. The autophagy effector Beclin 1: a novel BH3-only protein. Oncogene. 2008; 27(Suppl 1):S137–148. [PubMed: 19641499]
8. Wirawan E, Lippens S, Vanden Berghe T, Romagnoli A, Fimia GM, Piacentini M, Vandenabeele P. Beclin1: a role in membrane dynamics and beyond. Autophagy. 2012; 8:6–17. [PubMed: 22170155]
9. Hou W, Xie Y, Song X, Sun X, Lotze MT, Zeh HJ 3rd, Kang R, Tang D. Autophagy promotes ferroptosis by degradation of ferritin. Autophagy. 2016; 12:1425–1428. [PubMed: 27245739]
10. Gao M, Monian P, Pan Q, Zhang W, Xiang J, Jiang X. Ferroptosis is an autophagic cell death process. Cell Res. 2016; 26:1021–1032. [PubMed: 27514700]
11. He C, Wei Y, Sun K, Li B, Dong X, Zou Z, Liu Y, Kinch LN, Khan S, Sinha S, et al. Beclin 2 functions in autophagy, degradation of G protein-coupled receptors, and metabolism. Cell. 2013; 154:1085–1099. [PubMed: 23954414]
12. Petrat F, de Groot H, Rauen U. Determination of the chelatable iron pool of single intact cells by laser scanning microscopy. Arch Biochem Biophys. 2000; 376:74–81. [PubMed: 10729192]
13. Ayala A, Munoz MF, Arguelles S. Lipid peroxidation: production, metabolism, and signaling mechanisms of malondialdehyde and 4-hydroxy-2-nonenal. Oxid Med Cell Longev. 2014; 2014:360438. [PubMed: 24999379]
14. Xie Y, Zhu S, Song X, Sun X, Fan Y, Liu J, Zhong M, Yuan H, Zhang L, Billiar TR, et al. The Tumor Suppressor p53 Limits Ferroptosis by Blocking DPP4 Activity. Cell Rep. 2017; 20:1692–1704. [PubMed: 28813679]
15. Shoji-Kawata S, Sumpter R, Leveno M, Campbell GR, Zou Z, Kinch L, Wilkins AD, Sun Q, Pallauf K, MacDuff D, et al. Identification of a candidate therapeutic autophagy-inducing peptide. Nature. 2013; 494:201–206. [PubMed: 23364696]
16. Xie Y, Kang R, Sun X, Zhong M, Huang J, Klionsky DJ, Tang D. Posttranslational modification of autophagy-related proteins in macroautophagy. Autophagy. 2015; 11:28–45. [PubMed: 25484070]
17. Pattingre S, Tassa A, Qu X, Garuti R, Liang XH, Mizushima N, Packer M, Schneider MD, Levine B. Bcl-2 antiapoptotic proteins inhibit Beclin 1-dependent autophagy. Cell. 2005; 122:927–939. [PubMed: 16179260]
18. Kim J, Kim YC, Fang C, Russell RC, Kim JH, Fan W, Liu R, Zhong Q, Guan KL. Differential regulation of distinct Vps34 complexes by AMPK in nutrient stress and autophagy. Cell. 2013; 152:290–303. [PubMed: 23332761]

19. Lee Y, Park BH, Bae EJ. Compound C inhibits macrophage chemotaxis through an AMPK-independent mechanism. Biochem Biophys Res Commun. 2016; 469:515–520. [PubMed: 26682923]
20. Yang WS, SriRamaratnam R, Welsch ME, Shimada K, Skouta R, Viswanathan VS, Cheah JH, Clemons PA, Shamji AF, Clish CB, et al. Regulation of ferroptotic cancer cell death by GPX4. Cell. 2014; 156:317–331. [PubMed: 24439385]
21. Viswanathan VS, Ryan MJ, Dhruv HD, Gill S, Eichhoff OM, Seashore-Ludlow B, Kaffenberger SD, Eaton JK, Shimada K, Aguirre AJ, et al. Dependency of a therapy-resistant state of cancer cells on a lipid peroxidase pathway. Nature. 2017; 547:453–457. [PubMed: 28678785]
22. Alvarez SW, Sviderskiy VO, Terzi EM, Papagiannakopoulos T, Moreira AL, Adams S, Sabatini DM, Birsoy K, Possemato R. NFS1 undergoes positive selection in lung tumours and protects cells from ferroptosis. Nature. 2017; 551:639–643. [PubMed: 29168506]
23. Jiang L, Kon N, Li T, Wang SJ, Su T, Hibshoosh H, Baer R, Gu W. Ferroptosis as a p53-mediated activity during tumour suppression. Nature. 2015; 520:57–62. [PubMed: 25799988]
24. Sun X, Ou Z, Chen R, Niu X, Chen D, Kang R, Tang D. Activation of the p62-Keap1-NRF2 pathway protects against ferroptosis in hepatocellular carcinoma cells. Hepatology. 2016; 63:173–184. [PubMed: 26403645]
25. Zhu S, Zhang Q, Sun X, Zeh HJ 3rd, Lotze MT, Kang R, Tang D. HSPA5 Regulates Ferroptotic Cell Death in Cancer Cells. Cancer Res. 2017; 77:2064–2077. [PubMed: 28130223]
26. Sun X, Ou Z, Xie M, Kang R, Fan Y, Niu X, Wang H, Cao L, Tang D. HSPB1 as a novel regulator of ferroptotic cancer cell death. Oncogene. 2015; 34:5617–5625. [PubMed: 25728673]
27. Sun X, Niu X, Chen R, He W, Chen D, Kang R, Tang D. Metallothionein-1G facilitates sorafenib resistance through inhibition of ferroptosis. Hepatology. 2016; 64:488–500. [PubMed: 27015352]
28. Ingold I, Berndt C, Schmitt S, Doll S, Poschmann G, Buday K, Roveri A, Peng X, Porto Freitas F, Seibt T, et al. Selenium Utilization by GPX4 Is Required to Prevent Hydroperoxide-Induced Ferroptosis. Cell. 2018; 172:409–422 e421. [PubMed: 29290465]
29. Friedmann Angeli JP, Schneider M, Proneth B, Tyurina YY, Tyurin VA, Hammond VJ, Herbach N, Aichler M, Walch A, Eggenhofer E, et al. Inactivation of the ferroptosis regulator Gpx4 triggers acute renal failure in mice. Nature cell biology. 2014; 16:1180–1191. [PubMed: 25402683]
30. Matsushita M, Freigang S, Schneider C, Conrad M, Bornkamm GW, Kopf M. T cell lipid peroxidation induces ferroptosis and prevents immunity to infection. The Journal of experimental medicine. 2015; 212:555–568. [PubMed: 25824823]
31. Gao M, Monian P, Quadri N, Ramasamy R, Jiang X. Glutaminolysis and Transferrin Regulate Ferroptosis. Mol Cell. 2015; 59:298–308. [PubMed: 26166707]
32. Linkermann A, Skouta R, Himmerkus N, Mulay SR, Dewitz C, De Zen F, Prokai A, Zuchtriegel G, Krombach F, Welz PS, et al. Synchronized renal tubular cell death involves ferroptosis. Proceedings of the National Academy of Sciences of the United States of America. 2014; 111:16836–16841. [PubMed: 25385600]
33. Wang D, Peng Y, Xie Y, Zhou B, Sun X, Kang R, Tang D. Antiferroptotic activity of non-oxidative dopamine. Biochem Biophys Res Commun. 2016; 480:602–607. [PubMed: 27793671]
34. Yagoda N, von Rechenberg M, Zaganjor E, Bauer AJ, Yang WS, Fridman DJ, Wolpaw AJ, Smukste I, Peltier JM, Boniface JJ, et al. RAS-RAF-MEK-dependent oxidative cell death involving voltage-dependent anion channels. Nature. 2007; 447:864–868. [PubMed: 17568748]
35. Dixon SJ, Patel DN, Welsch M, Skouta R, Lee ED, Hayano M, Thomas AG, Gleason CE, Tatonetti NP, Slusher BS, et al. Pharmacological inhibition of cystine-glutamate exchange induces endoplasmic reticulum stress and ferroptosis. eLife. 2014; 3:e02523. [PubMed: 24844246]
36. Chen D, Tavana O, Chu B, Erber L, Chen Y, Baer R, Gu W. NRF2 Is a Major Target of ARF in p53-Independent Tumor Suppression. Mol Cell. 2017; 68:224–232 e224. [PubMed: 28985506]
37. Kroemer G, Levine B. Autophagic cell death: the story of a misnomer. Nature reviews. Molecular cell biology. 2008; 9:1004–1010. [PubMed: 18971948]
38. Marino G, Niso-Santano M, Baehrecke EH, Kroemer G. Self-consumption: the interplay of autophagy and apoptosis. Nat Rev Mol Cell Biol. 2014; 15:81–94. [PubMed: 24401948]
39. Liu Y, Levine B. Autosis and autophagic cell death: the dark side of autophagy. Cell death and differentiation. 2015; 22:367–376. [PubMed: 25257169]

40. Niso-Santano M, Bravo-San Pedro JM, Maiuri MC, Tavernarakis N, Cecconi F, Madeo F, Codogno P, Galluzzi L, Kroemer G. Novel inducers of BECN1-independent autophagy: cis-unsaturated fatty acids. Autophagy. 2015; 11:575–577. [PubMed: 25714112]

41. Al Dhaheri Y, Attoub S, Ramadan G, Arafat K, Bajbouj K, Karuvantevida N, AbuQamar S, Eid A, Iratni R. Carnosol induces ROS-mediated beclin1-independent autophagy and apoptosis in triple negative breast cancer. PloS one. 2014; 9:e109630. [PubMed: 25299698]

42. Huang W, Choi W, Hu W, Mi N, Guo Q, Ma M, Liu M, Tian Y, Lu P, Wang FL, et al. Crystal structure and biochemical analyses reveal Beclin 1 as a novel membrane binding protein. Cell research. 2012; 22:473–489. [PubMed: 22310240]

43. Liang C, Feng P, Ku B, Dotan I, Canaani D, Oh BH, Jung JU. Autophagic and tumour suppressor activity of a novel Beclin1-binding protein UVRAG. Nature cell biology. 2006; 8:688–699. [PubMed: 16799551]

44. Zalckvar E, Berissi H, Mizrachy L, Idelchuk Y, Koren I, Eisenstein M, Sabanay H, Pinkas-Kramarski R, Kimchi A. DAP-kinase-mediated phosphorylation on the BH3 domain of beclin 1 promotes dissociation of beclin 1 from Bcl-XL and induction of autophagy. EMBO reports. 2009; 10:285–292. [PubMed: 19180116]

45. Zhang D, Wang W, Sun X, Xu D, Wang C, Zhang Q, Wang H, Luo W, Chen Y, Chen H, et al. AMPK regulates autophagy by phosphorylating BECN1 at threonine 388. Autophagy. 2016; 12:1447–1459. [PubMed: 27304906]

46. Huo H, Zhou Z, Qin J, Liu W, Wang B, Gu Y. Erastin Disrupts Mitochondrial Permeability Transition Pore (mPTP) and Induces Apoptotic Death of Colorectal Cancer Cells. PLoS One. 2016; 11:e0154605. [PubMed: 27171435]

47. Song X, Zhu S, Xie Y, Liu J, Sun L, Zeng D, Wang P, Ma X, Kroemer G, Bartlett DL, et al. JTC801 Induces pH-dependent Death Specifically in Cancer Cells and Slows Growth of Tumors in Mice. Gastroenterology. 2017

48. Xie Y, Zhu S, Zhong M, Yang M, Sun X, Liu J, Kroemer G, Lotze M, Zeh HJ 3rd, Kang R, et al. Inhibition of Aurora Kinase A Induces Necroptosis in Pancreatic Carcinoma. Gastroenterology. 2017; 153:1429–1443 e1425. [PubMed: 28764929]

49. Torres MP, Rachagani S, Souchek JJ, Mallya K, Johansson SL, Batra SK. Novel pancreatic cancer cell lines derived from genetically engineered mouse models of spontaneous pancreatic adenocarcinoma: applications in diagnosis and therapy. PloS one. 2013; 8:e80580. [PubMed: 24278292]

50. Yu Y, Xie Y, Cao L, Yang L, Yang M, Lotze MT, Zeh HJ, Kang R, Tang D. The ferroptosis inducer erastin enhances sensitivity of acute myeloid leukemia cells to chemotherapeutic agents. Mol Cell Oncol. 2015; 2:e1054549. [PubMed: 27308510]

Highlights

- BECN1 is required for system X_c^- inhibitor-induced ferroptosis
- BECN1 inhibits system Xc^- activity through directly binding to SLC7A11
- AMPK is required for BECN1 phosphorylation in ferroptosis
- BECN1 contributes to the anticancer activity of ferroptosis *in vivo*

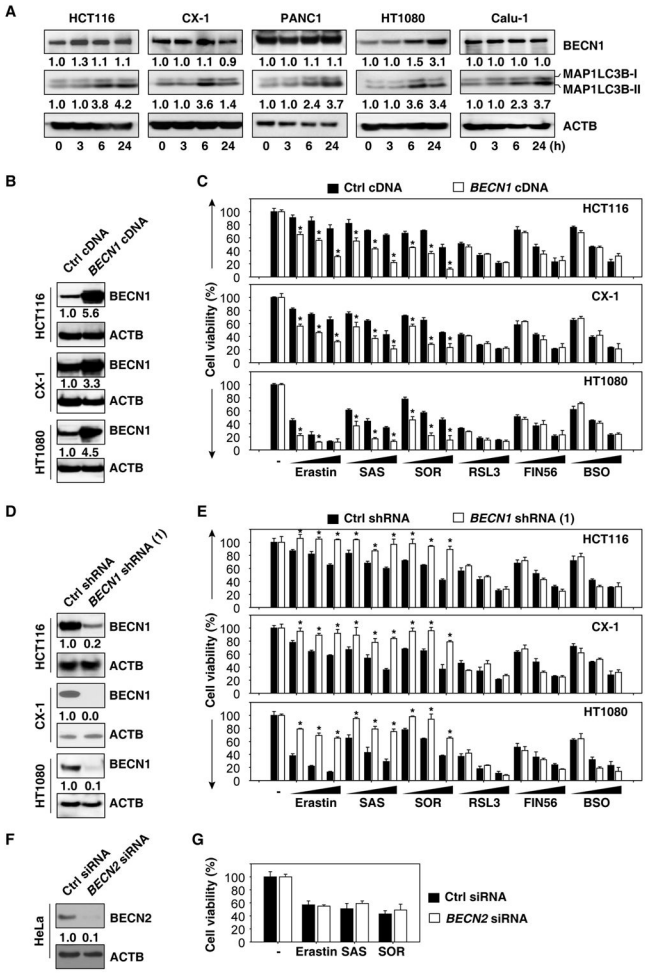

Figure 1. BECN1 is required for system X_c^- inhibitor-induced ferroptosis

(**A**) Effects of erastin on the expression of indicated proteins in HCT116 (20 μM), CX-1 (20 μM), PANC1 (10 μM), HT1080 (5 μM), and Calu-1 (10 μM) cells. (**B**) Western blot analysis of BECN1 expression in BECN1-overexpressing cells. (**C**) Overexpression of BECN1 increased erastin (20 μM for HCT116 and CX-1 cells; 5 μM for HT1080 cells)-, sulfasalazine ("SAS", 1 mM)-, and sorafenib ("SOR", 10 μM)-induced cell death, but not RSL3 (1 μM)-, FIN56 (5 μM)-, and buthionine sulfoximine ("BSO", 100 μM)-induced cell death at 24, 48, and 72 h (n=3, *, P<0.05 versus control group, t test). (**D**) Western blot analysis of BECN1 expression in BECN1-knockdown cells. (**E**) Knockdown of BECN1 inhibited erastin (20 μM for HCT116 and CX-1 cells; 5 μM for HT1080 cells)-, sulfasalazine ("SAS", 1 mM)-, and sorafenib ("SOR", 10 μM)-induced cell death, but not RSL3 (1 μM)-, FIN56 (5 μM)- and buthionine sulfoximine ("BSO", 100 μM)-induced cell death at 24, 48, and 72 h (n=3, *, P<0.05 versus control group, t test). (**F**) Western blot analysis of BECN2 expression in BECN2-knockdown HeLa cells. (**G**) Indicated HeLa cells were treated with erastin (20 μM), sulfasalazine ("SAS", 1 mM), and sorafenib ("SOR", 10 μM) for 24 h and cell viability were assayed. See also Figures S1 and S2.

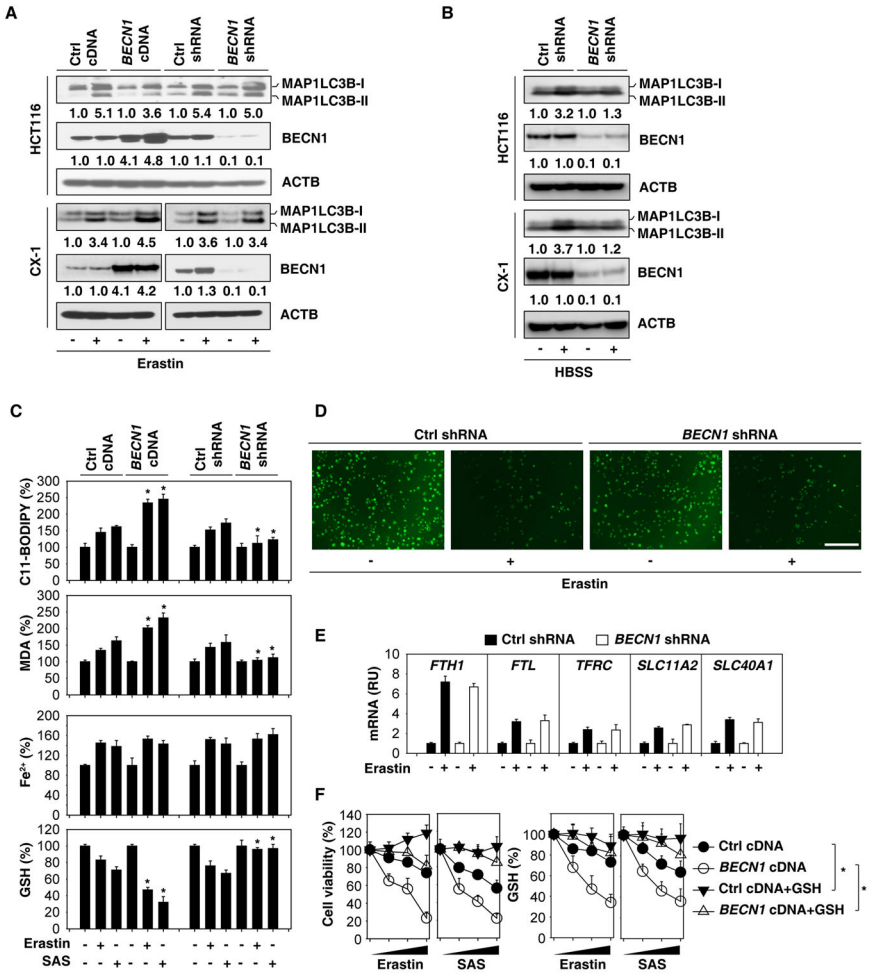

Figure 2. BECN1 promotes GSH depletion and lipid peroxidation in ferroptosis

(**A**) Indicated HCT116 and CX-1 cells were treated with erastin (20 μM) for 24 h. The protein levels of MAP1LC3B were assayed. (**B**) The indicated HCT116 and CX-1 cells were treated with HBSS for 6 h. The protein levels of MAP1LC3B were assayed. (**C**) The indicated HCT116 cells were treated with erastin (20 μM) or sulfasalazine (“SAS”, 1 mM) for 24 h. The relative levels of C11-BODIPY, MDA, Fe^{2+}, and GSH were assayed (n=3, *, P<0.05 versus control group, t test). **(D)** Intracellular chelatable iron in indicated HT1080 cells treated with or without erastin (5 μM, 24 h) was determined using the fluorescent indicator Phen Green SK (green). **(E)** Q-PCR analysis of gene expression in indicated HT1080 cells treated with or without erastin (5 μM, 24 h). RU=relative units. (**F**) Administration of GSH (5 mM) restored intracellular GSH level and inhibited erastin (20 μM)- or sulfasalazine (“SAS”, 1 mM)-induced cell death at 24–72 h in wild-type and *BECN1*-overexpressing HCT116 cells. See also Figure S3.

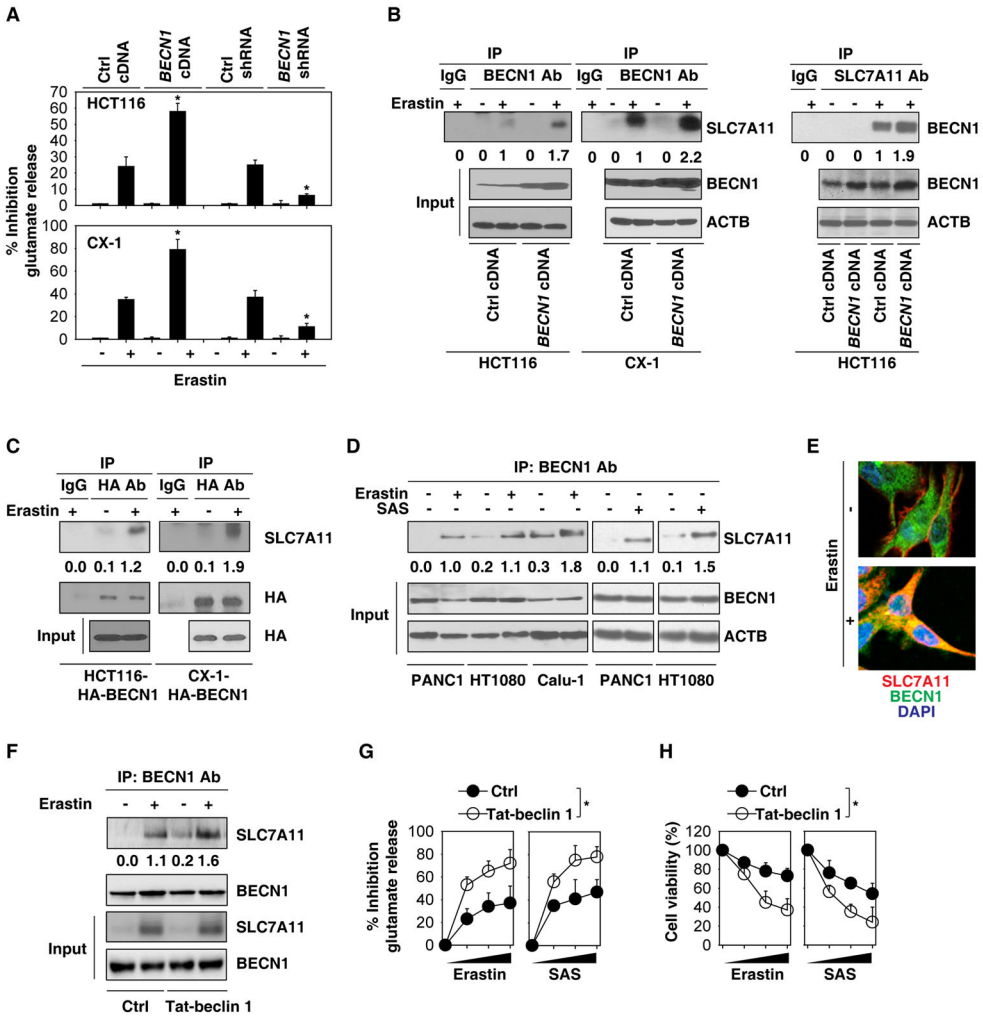

Figure 3. BECN1 inhibits system Xc⁻ activity through direct binding to SLC7A11

(**A**) Analysis of glutamate release from the indicated cells in response to erastin (20 μM) for 24 h (n=3, *, $P<0.05$ versus control group, *t* test). (**B**) IP analysis of BECN1-SLC7A11 formation in the indicated cells following erastin (20 μM) treatment for 24 h. (**C**) IP analysis of BECN1-SLC7A11 formation in the indicated cells following erastin (20 μM) treatment for 24 h. (**D**) IP analysis of BECN1-SLC7A11 formation in the indicated cells following erastin (10 μM for PANC1 cells; 5 μM for HT1080 cells; 10 μM for Calu-1 cells) or sulfasalazine ("SAS", 1 mM) treatment for 24 h. **(E)** Image assay showed that the colocalization between BECN1 (green) and SLC7A11 (red) in cytoplasm in CX-1 cells following erastin (20 μM) treatment for 24 h. Nucleus were stain by DAPI (blue). (**F**) IP analysis of BECN1-SLC7A11 formation in HCT116 cells following erastin (20 μM) treatment with or without Tat-beclin 1 (10 μM) for 24 h. (**G**) Analysis of glutamate release from HCT116 cells in response to erastin (20 μM) or sulfasalazine ("SAS", 1 mM) with or without Tat-beclin 1 (10 μM) and control peptides (10 μM) for 24–72 h (n=3, *, $P<0.05$, ANOVA test). (**H**) Analysis of cell viability from HCT116 cells in response to erastin (20 μM) or sulfasalazine ("SAS", 1 mM) with or without Tat-beclin 1 (10 μM) control peptides (10 μM) for 24–72 h (n=3, *, $P<0.05$, ANOVA test). See also Figure S4.

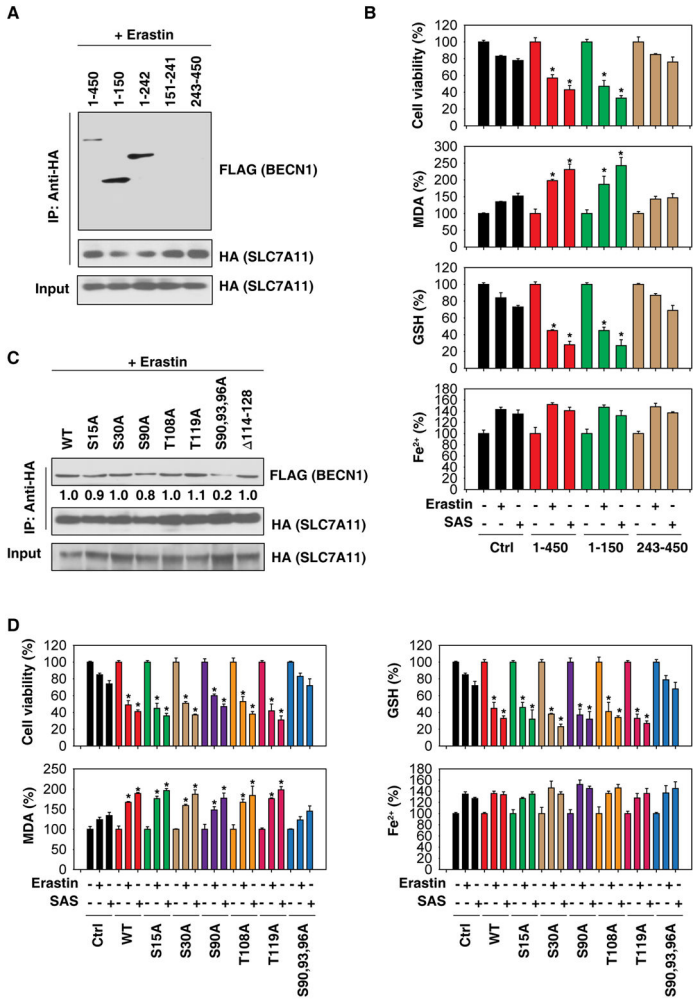

Figure 4. BECN1 phosphorylation at S90/93/96 contributes to BECN1-SLC7A11 complex formation

(**A**) IP analysis of BECN1-SLC7A11 formation in HEK293T cells expressing HA-SLC7A11-cDNA and the indicated FLAG-BECN1 mutants following erastin (20 μM) treatment for 24 h. (**B**) The levels of cell viability, MDA, GSH, and Fe2+ were assayed in HEK293T cells expressing the indicated FLAG-BECN1 mutants following erastin (20 μM) or sulfasalazine (“SAS”, 1 mM) treatment for 24 h (n=3, *, $P<0.05$ versus control group, *t* test). (**C**) IP analysis of BECN1-SLC7A11 formation in HEK293T cells expressing HA-SLC7A11-cDNA and the indicated FLAG-BECN1 mutants following erastin (20 μM) treatment for 24 h. (**D**) The levels of cell viability, MDA, GSH, and Fe2+ were assayed in HEK293T cells expressing the indicated BECN1 mutants following erastin (20 μM) or sulfasalazine (“SAS”, 1 mM) treatment for 24 h (n=3, *, $P<0.05$ versus control group, *t* test).

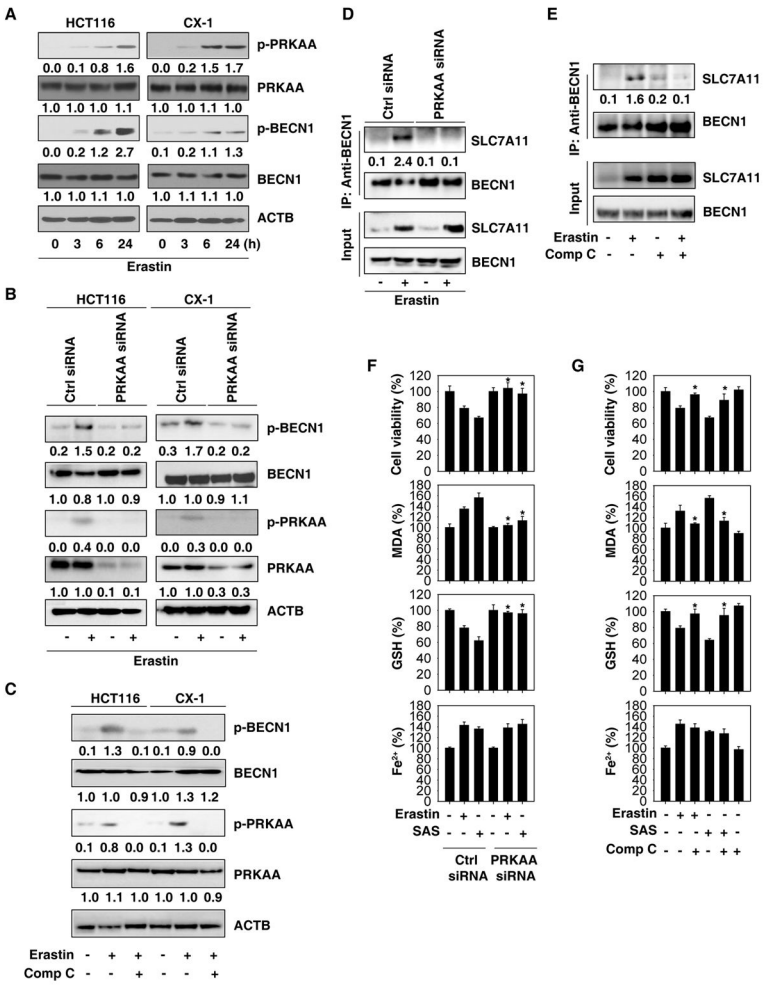

Figure 5. AMPK is required for BECN1 phosphorylation in ferroptosis

(**A**) Western blot analysis of phosphorylation of PRKAA/AMPKα and BECN1 in HCT116 and CX-1 cells following erastin (20 μM) treatment for 3 to 24 h. (**B**) Knockdown of PRKAA/AMPKα inhibited erastin (20 μM, 24 h)-induced BECN1 phosphorylation in HCT116 and CX-1 cells. (**C**) Compound C (Comp C, 1 μM) inhibited erastin (20 μM, 24 h)-induced BECN1 phosphorylation in HCT116 and CX-1 cells. (**D**) Knockdown of PRKAA/AMPKα inhibited erastin (20 μM, 24 h)-induced BECN1-SLC7A11 complex formation in HCT116 cells. (**E**) Compound C (1 μM) inhibited erastin (20 μM, 24 h)-induced BECN1-SLC7A11 complex formation in HCT116 cells. (**F**) Analysis of the levels of cell viability, MDA, GSH, and Fe^{2+} in the indicated HCT116 cells following erastin (20 μM) or sulfasalazine (SAS, 1 mM) treatment for 24 h (n=3, *, P<0.05 versus control group, t test). (**G**) Analysis of the levels of cell viability, MDA, GSH, and Fe^{2+} in HCT116 cells following erastin (20 μM) or sulfasalazine (1 mM) treatment with or without compound C (1 μM) for 24 h (n=3, *, P<0.05 versus erastin or SAS group, t test). See also Figure S5.

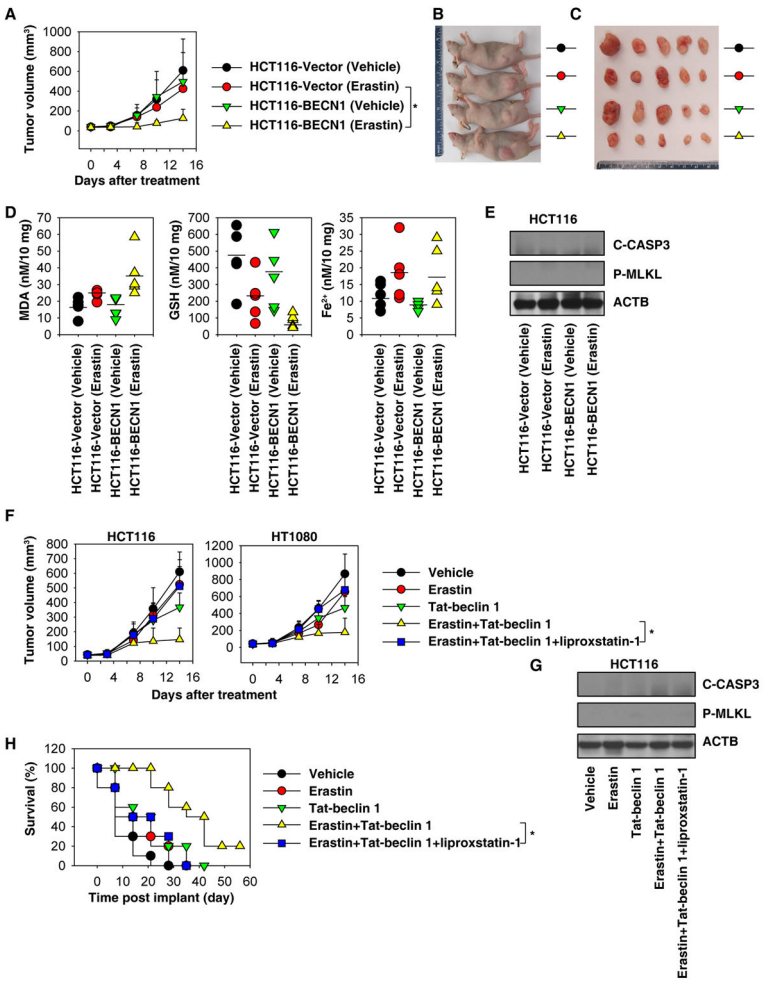

Figure 6. BECN1 contributes to the anticancer activity of erastin *in vivo*

(**A**) Athymic nude mice were injected subcutaneously with the indicated HCT116 cells and treated with erastin (40 mg/kg/intraperitoneal injection, once every day) at day 7 for two weeks. Tumor volume was calculated weekly (n=5 mice/group, * $p < 0.05$, ANOVA *LSD* test). (**B, C**) Representative photographs of tumor-bearing mice and isolated tumors at day 14 after treatment. (**D**) In parallel, MDA, GSH, and Fe^{2+} levels in isolated tumors at day 14 after treatment were assayed (n=5 mice/group). **(E)** Western blot analysis of cleaved-CASP3 and p-MLKL in isolated tumors at day 14 after treatment from (A). (**F**) Athymic nude mice were injected subcutaneously with HCT116 or HT1080 cells for seven days and then treated with the indicated erastin (40 mg/kg/intraperitoneal [i.p.] injection, once every day), Tat-beclin 1 (20 mg/kg/i.p. injection, once every day), or liprostatin-1 (10 mg/kg/i.p. injection, once every day) at day 7 for two weeks. Tumor volume was calculated weekly (n=5 mice/group, * $p < 0.05$, ANOVA test). **(G)** Western blot analysis of cleaved-CASP3 and p-MLKL in isolated tumors at day 14 after treatment from (F). (**H**) KPC cells were surgically implanted into the pancreases in B6 mice for seven days and then treated with erastin (40 mg/kg/i.p. injection, once every day), Tat-beclin 1 (20 mg/kg/i.p. injection, once every day), or liprostatin-1 (10 mg/kg/i.p. injection, once every day) at day 7 for two weeks. Animal

survival was calculated weekly (n=10 mice/group, Kaplan-Meier survival analysis, * $p < 0.05$). See also Figure S6.

KEY RESOURCES TABLE

REAGENT or RESOURCE	SOURCE	IDENTIFIER
Antibodies		
Rabbit anti-ATG5 (D5F5U) monoclonal antibody	Cell Signaling Technology	Cat#12994, RRID:AB_2630393
Rabbit anti-HA-Tag (C29F4) monoclonal antibody	Cell Signaling Technology	Cat#3724, RRID:AB_1549585
Rabbit anti-DYKDDDDK Tag (D6W5B) monoclonal antibody	Cell Signaling Technology	Cat#14793, RRID:AB_2572291
Rabbit anti-PI3 kinase class III (D9A5) monoclonal antibody	Cell Signaling Technology	Cat#4263, RRID:AB_2299765
Rabbit anti-phospho-AMPKα (Thr172) (40H9) monoclonal antibody	Cell Signaling Technology	Cat#2535, RRID:AB_331250
Rabbit anti-AMPK (D63G4) monoclonal antibody	Cell Signaling Technology	Cat#5832, RRID:AB_1062486
Rabbit anti-phospho-Beclin1 (Ser93) (D9A5G) monoclonal antibody	Cell Signaling Technology	Cat#14717, RRID: AB_2688032
Rabbit anti-cleaved caspase-3 (Asp175) (5A1E) monoclonal antibody	Cell Signaling Technology	Cat#9664, RRID: AB_2070042
Rabbit anti-phospho-MLKL (Ser358) (D6H3V) monoclonal antibody	Cell Signaling Technology	Cat#91689, RRID: N/A
Rabbit anti-Beclin2 polyclonal antibody	Novus Biologicals	Cat# NB110-60984, RRID: AB_925724
Rabbit anti-LC3B (D11) monoclonal antibody	Cell Signaling Technology	Cat#3868, RRID:AB_2137707
Rabbit anti-GPX4 (EPNCIR144) monoclonal antibody	Abcam	Cat#ab125066, RRID:AB_10973901
Mouse anti-β-actin (AC-15) monoclonal antibody	Sigma-Aldrich	Cat#A5441, RRID:AB_476744
Rabbit anti-Beclin1 (D40C5) monoclonal antibody	Cell Signaling Technology	Cat#3495, RRID:AB_1903911
Mouse anti-Beclin1 monoclonal antibody (clone 20)	BD Biosciences	Cat#612113, RRID:AB_399484
Rabbit anti-xCT/SLC7A11 (D2M7A) monoclonal antibody	Cell Signaling Technology	Cat#12691, RRID:AB_2687474
Rabbit anti-xCT/SLC7A11 polyclonal antibody	Abcam	Cat#ab37185, RRID:AB_778944
Anti-mouse IgG, HRP-linked antibody	Cell Signaling Technology	Cat#7076, RRID:AB_330924
Anti-rabbit IgG, HRP-linked antibody	Cell Signaling Technology	Cat#7074, RRID:AB_2099233
Goat anti-rabbit IgG (H+L) secondary antibody, Alexa fluor 488 conjugate	Thermo Fisher Scientific	Cat#R37116, RRID:AB_2556544
Goat anti-rabbit IgG (H+L) secondary antibody, Cyanine3 conjugate	Thermo Fisher Scientific	Cat# A10520, RRID: AB_2534029
Donkey anti-mouse IgG (H+L) secondary antibody, Alexa fluor 488 conjugate	Thermo Fisher Scientific	Cat# A-21202, RRID: AB_141607
Chemicals, Peptides, and Recombinant Proteins		
Cycloheximide	Sigma-Aldrich	C4859
Necrosulfonamide	Sigma-Aldrich	480073
Protease inhibitor cocktail	Sigma-Aldrich	P8340
Puromycin	Sigma-Aldrich	P9620

REAGENT or RESOURCE	SOURCE	IDENTIFIER
Z-VAD-FMK	Sigma-Aldrich	V116
TNF	Sigma-Aldrich	T6674
Compound C	Sigma-Aldrich	171260
Sulfasalazine	Sigma-Aldrich	1636005
Buthionine sulfoximine	Sigma-Aldrich	B2515
Staurosporine	Sigma-Aldrich	37095
Erastin	Selleck Chemicals	S7242
RSL3	Selleck Chemicals	S8155
FIN56	Selleck Chemicals	S8254
Ferrostatin-1	Selleck Chemicals	S7243
Liproxstatin-1	Selleck Chemicals	S7699
Sorafenib	Selleck Chemicals	S7397
Phosphate buffered saline	Thermo Fisher Scientific	AM9625
Cell lysis buffer	Cell Signaling Technology	9803
4%-12% Criterion XT Bis-Tris gel	Bio-Rad	3450124
XT MES running buffer	Bio-Rad	1610789
PVDF membranes	Bio-Rad	1620233
TBST	Cell Signaling Technology	9997S
SuperSignal™ West Pico Chemiluminescent Substrate	Thermo Fisher Scientific	34080
SuperSignal™ West Femto Maximum Sensitivity Substrate	Thermo Fisher Scientific	34095
Protein A agarose beads	Santa Cruz Biotechnology	sc-2027
DAPI	Thermo Fisher Scientific	H3569
Propidium iodide	Sigma-Aldrich	P4170
Phen Green™ SK	Thermo Fisher Scientific	P14313
Gateway LR Clonase II enzyme mix	Thermo Fisher Scientific	11791100
3rd Generation Packaging Mix	Abm	LV053
ssoFast EvaGreen Supermix	Bio-Rad	172-5204
Lipofectamine 3000	Thermo Fisher Scientific	L3000-015
C11-BODIPY dye	Thermo Fisher Scientific	D3861
Tat-beclin 1	Millipore	5.06048.0001
Inactive/scrambled control peptides	Millipore	5.31038.0001
Critical Commercial Assays		
BCA assay kit	Thermo Fisher Scientific	23225
Cell counting kit-8 kit	Dojindo Laboratories	CK04
QuikChange site-directed mutagenesis kit	Agilent Technologies	200523
pENTER-D-TOPO kit	Thermo Fisher Scientific	K240020
RNeasy plus mini kit	QIAGEN	74136
iScript cDNA synthesis kit	Bio-Rad	170-8891

REAGENT or RESOURCE	SOURCE	IDENTIFIER
Amplex red glutamate release assay Kit	Thermo Fisher Scientific	A12221
Glutathione assay kit	Sigma-Aldrich	CS0260
Lipid peroxidation (MDA) assay kit	Abcam	ab118970
Iron assay kit	Sigma-Aldrich	MAK025
Experimental Models: Cell Lines		
HCT116	ATCC	CCL-247
PANC1	ATCC	CCL-1469
HT1080	ATCC	CCL-121
Calu-1	ATCC	HTB-54
HEK293T	ATCC	CRL-3216
HeLa	ATCC	CCL-2
CX-1	Dr. Yong Lee Lab	N/A
Mouse PDAC cell line KPC	KPC mice (*Pdx1-Cre;K-Ras$^{G12D/+}$;Trp53$^{R172H/+}$*)	N/A
Experimental Models: Organisms/Strains		
Athymic nude	Charles River	Cat#490
C57BL6/J mice	Charles River	Cat#27
Oligonucleotides		
Human PRKAA1/AMPKα1 siRNA: 5′-AGUGAAGGUUGGCAAACAU-3′ (sense strand) and 5′-AUGUUUGCCAACCUUCACU-3′ (complement strand)	Sigma-Aldrich	This paper
Human PRKAA2/AMPKα2 siRNA: 5′-GGAAGGUAGUGAAUGCAUA-3′ (sense strand) and 5′-UAUGCAUUCACUACCUUCC-3′ (complement strand)	Sigma-Aldrich	This paper
Human BECN2 siRNA pools	Santa Cruz Biotechnology	sc-88199
Control siRNA	Sigma-Aldrich	SIC001
See Table S2 for primers used for mutant and qPCR	This paper	Table S1
Recombinant DNA		
PcDNA4-Becn1	Addgene	24388
pLenti CMV Puro DEST	Addgene	17452
Human-Slc7a11-cDNA	GeneCopoeia	EX-U1104-Lv120
PcDNA4-Becn1 1-242	Addgene	24391
PcDNA4-Becn1 151-241	Addgene	24393
PcDNA4-Becn1 1-150	Addgene	24389
PcDNA4-Becn1 243-450	Addgene	24392
Control empty shRNA	Sigma-Aldrich	#SHC001
Human-BECN1-shRNA-1	Sigma-Aldrich	TRCN0000299864
Human-BECN1-shRNA-2	Sigma-Aldrich	TRCN0000299789
Human-BECN1-shRNA-3	Sigma-Aldrich	TRCN0000299790

REAGENT or RESOURCE	SOURCE	IDENTIFIER
Human-ATG5-shRNA	Sigma-Aldrich	TRCN0000151963
Software and Algorithms		
Image Lab™ software	Bio-Rad	http://www.bio-rad.com/en-us/product/image-lab-software?ID=KRE6P5
CFX Manager software	Bio-Rad	http://www.bio-rad.com/en-us/sku/1845000-cfx-manager-software?ID=1
Prism 7	GraphPad	https://www.graphpad.com/scientific-software/prism/